Chemical Vapor Deposition

Full Paper

Atomic Layer Deposition of Hafnium Dioxide Films from Hafnium Tetrakis(ethylmethylamide) and Water**

By *Kaupo Kukli*,* *Mikko Ritala*, *Timo Sajavaara*, *Juhani Keinonen*, and *Markku Leskelä*

HfO_2 films were produced from $Hf[N(CH_3)(C_2H_5)]_4$ and H_2O, on borosilicate glass, indium-tin-oxide (ITO), and Si(100) substrates, in the temperature range 150–325 °C, using atomic layer deposition (ALD). In the temperature range 200–250 °C, the growth rate of the HfO_2 films was 0.09 nm per cycle, but increased with both increasing and decreasing temperatures. The self-limiting adsorption of $Hf[N(CH_3)(C_2H_5)]_4$ at 250 °C was verified. The films were stoichiometric dioxides with an O/Hf ratio of 2.0 ± 0.1. The concentrations of residual carbon, nitrogen, and hydrogen, determined using ion beam analysis, were 0.3–0.6 at.-%, 0.1–0.2 at.-%, and 2–3 at.-%, respectively. The films crystallized at growth temperatures exceeding 150–175 °C, and consisted mainly of the monoclinic HfO_2 phase. The refractive index of the films varied between 2.08 and 2.10. The effective permittivities of the HfO_2 films grown in the temperature range 200–300 °C varied between 11 and 14.

Keywords: Atomic layer deposition, Dielectrics, Hafnium dioxide, Ion beam analysis

1. Introduction

HfO_2 is a potential candidate for several applications such as high-permittivity dielectric oxide in metal oxide semiconductor (MOS) devices,[1–3] thin film capacitors,[4] gas-sensing devices,[5] tunnel junctions,[6] and laser damage-resistant optical coatings.[7] The maximum dielectric constant value for HfO_2 (30) may exceed that of ZrO_2 (25),[8] another prospective candidate for metal oxide semiconductor field effect transistor (MOSFET) gate oxides.[3] However, relatively low values (15.7 ± 0.5, measured at 100 kHz) of the dielectric constant have been reported for HfO_2 films.[9] The optical energy gap is reported to be higher in HfO_2, compared to ZrO_2.[5,10] The refractive index of HfO_2 films is in the range 2.08–2.15,[7–9,11] slightly lower than that of ZrO_2 (2.2).[8]

HfO_2 thin films have often been grown using physical vapor deposition methods, such as sputtering or e-beam evaporation,[6–9,12–15] while in the CVD routes to HfO_2 films, β-diketonate precursors have been exploited.[16,17] In recent studies, the use of hafnium nitrate, $Hf(NO_3)_4$,[1,18] and hafnium tetrakis(diethylamide), $Hf[N(C_2H_5)_2]_4$,[19,20] were described.

Hafnium halides, especially $HfCl_4$, have been the common Hf precursors in the ALD process. In ALD, a substrate surface is alternately exposed to highly reactive metal and oxygen precursors, and the solid film forms as a result of successive surface reactions between (sub)monolayers of precursor molecules alternately adsorbed. $HfCl_4$ and H_2O have been applied to grow binary HfO_2,[2,11,21,22] or HfO_2-Ta_2O_5 nanolaminate films.[4,23] Recently, HfI_4 and H_2O-H_2O_2 have also been applied in an ALD process.[24] The permittivity of the 150–170 nm thick films grown from $HfCl_4$ and H_2O at 325 °C on ITO substrates was 16, measured at 10 kHz.[23] The refractive index of ALD HfO_2 films was 2.10, measured at 580 nm.[11] Gordon et al.[25] have noted that it is possible to grow HfO_2 films in ALD mode from hafnium tetrakis(dimethylamide), and H_2O, with a growth rate of 0.1 nm per cycle. However, the properties of these films were not described. It is to be noted that the reproducibility of HfO_2 capacitors grown from $HfCl_4$ may sometimes suffer from particle transport, originating from the hafnium precursor,[11] therefore the exploitation of liquid precursors, ensuring uniform precursor delivery, is recommended.

In the present study, HfO_2 films were grown by ALD from a novel hafnium precursor, hafnium tetrakis(ethylmethylamide), and H_2O in order to investigate the basic features of the film growth in this new precursor combination. The dependence of the growth rate on the substrate temperature and ALD cycle time parameters was investigated. In addition, the effect of substrate temperature on the film structure and composition will be described. Preliminary results on the dielectric properties of the films grown at various temperatures will be reported.

[*] Dr. K. Kukli,[+] Dr. M. Ritala, Prof. M. Leskelä
Department of Chemistry University of Helsinki
P.O. Box 55 (A.I.Virtasen aukio 1)
FIN-00014 University of Helsinki (Finland)
E-mail: kukli@pcu.helsinki.fi
Dr. T. Sajavaara, Prof. J. Keinonen
Accelerator Laboratory, University of Helsinki
P.O. Box 43, FIN-00014 University of Helsinki (Finland)
[+] Second address: Institute of Experimental Physics and Technology, University of Tartu, Tähe 4, EE-51010 Tartu, Estonia.
E-mail: kaupok@ut.ee.

[**] The study was supported by the Academy of Finland (Projects Nos. 51989, 43329 and 44215).

  0948-1907/02/0509-0199 $ 17.50+.50/0

2. Results and Discussion

2.1. Film Growth

The length of the $Hf[N(CH_3)(C_2H_5)]_4$ pulse was varied at 250 °C in order to study the self-limiting nature of the $Hf[N(CH_3)(C_2H_5)]_4$ adsorption. Figure 1 shows that a pulse length of 0.4 s was sufficient to achieve maximum growth rate, no marked increase in the growth rate being

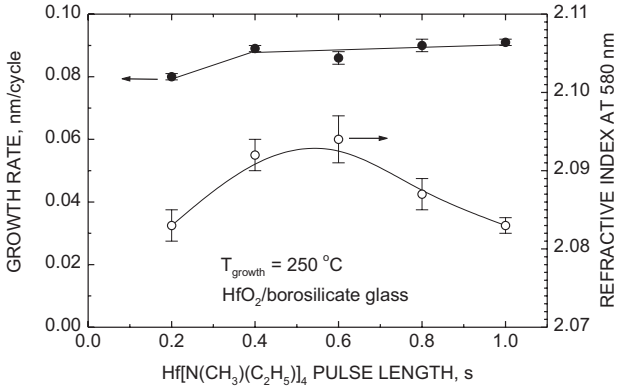

Fig. 1. Growth rate and refractive index of HfO_2 films as a function of hafnium precursor pulse length. The water pulse and purge times were 0.5 s. The error bars express the variation of the refractive index in each sample.

observed for greater pulse lengths. It can also be seen that the refractive index of the resulting films reaches maximum value in the $Hf[N(CH_3)(C_2H_5)]_4$ pulse length range 0.4–0.6 s, while increasing the pulse length somewhat reduces the refractive index. This can arise from the thermal decomposition of $Hf[N(CH_3)(C_2H_5)]_4$, which may become more significant during longer exposure times, slightly reducing the film density or changing the film composition. It is to be noted that the changes in refractive index are very small, although clearly measurable. In most of the depositions, the $Hf[N(CH_3)(C_2H_5)]_4$ pulse length was 0.4 s.

Figure 2 depicts the thickness profiles of the films grown on glass substrates. It can be seen that the films show quite

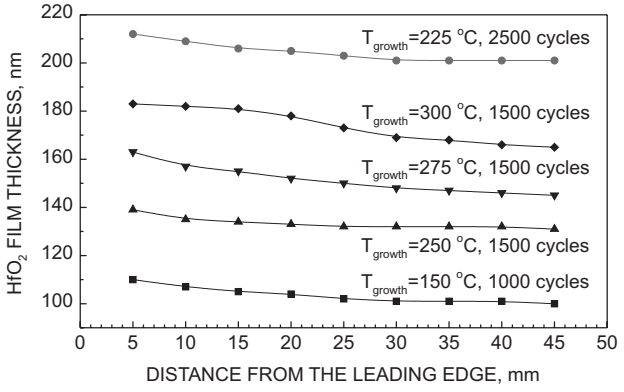

Fig. 2. Thickness profile of selected HfO_2 films grown from $Hf[N(CH_3)(C_2H_5)]_4$ and H_2O on borosilicate glass substrates. Growth temperatures and numbers of growth cycles applied are indicated by labels. Thicknesses are measured at variable distance from the leading edge of the substrate, which is the edge closest to the precursor inlet.

uniform thickness over a large substrate area. Somewhat decreased uniformity can be observed at 275 °C and above, very possibly indicating an increasing effect of the thermal decomposition of $Hf[N(CH_3)(C_2H_5)]_4$. It is to be noted that HfO_2 films of similar uniformity can be grown by ALD from $HfCl_4$ and H_2O at 500 °C,[11] but the application of lower growth temperatures in the case of $HfCl_4$ has resulted in a stronger thickness profile exceeding 10–15 % deviations over the substrate.

In Figure 3, the film growth rate and refractive index are plotted against the substrate temperature. It is obvious that between 200 °C and 250 °C the growth rate is almost inde-

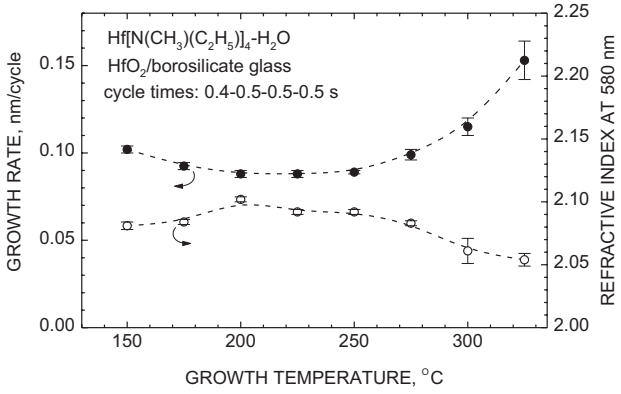

Fig. 3. Growth rate and refractive index of HfO_2 films as a function of growth temperature.

pendent of the growth temperature. In this range, the adsorption of $Hf[N(CH_3)(C_2H_5)]_4$ molecules may be expected to be a self-limiting process during 0.4 s long precursor pulses. In the case of self-limitation and absence of thermal decomposition, adsorption proceeds until all the reactive, functional groups on the surface (such as –OH groups) are used up.

A separate experiment was carried out to examine the thermal decomposition of the hafnium precursor. $Hf[N(CH_3)(C_2H_5)]_4$ was pulsed 1500–2750 times with a pulse length of 0.6 s and without an intermittent hydrolysis step, i.e., a water pulse. At 205 °C, film growth was negligible. At 250 °C, ultrathin, brownish layers of unknown composition were formed on the glass substrates, indicating weak thermal decomposition. Thus, the growth cannot be expected to be perfectly self-limiting. The increase in growth rate at lower temperatures may be due to the increased density of functional adsorption sites (–OH groups) or the molecular adsorption of the precursor. At higher temperatures, the growth rate can be enhanced by intense thermal decomposition of the hafnium precursor.

The growth rate of the films in the present study increases rather rapidly from 0.09 nm per cycle at 250 °C to 0.15 nm per cycle at 325 °C, while the growth rate reported for the $Hf[N(CH_3)_2]_4$ and H_2O precursors[25] was about 0.1 nm per cycle in the temperature range 250–350 °C. The difference in growth rates may be connected, no only to the properties of Hf precursors, but also to differences in

  0948-1907/02/0509-0200 $ 17.50+.50/0

gas flow rate and processing time parameters, depending on the reactor used. In terms of precursor properties, $Hf[N(CH_3)(C_2H_5)]_4$ is more volatile than $Hf[N(CH_3)_2]_4$, but can also be somewhat less stable at higher temperatures. However, considering the interatomic distances in HfO_2 (0.2086–0.2197 nm for Hf–O and 0.3547–0.3386 nm for Hf–Hf)[26] as well as the lattice parameters,[27] it is still obvious that the average growth rate remains below one monolayer of hafnium oxide.

The refractive index of HfO_2, measured in this study, agrees with the literature values.[7–9,13–15] From Figure 3, it can be seen that the maximum values of refractive index coincide with the region of temperature-independent growth rate, whereas too low or too high temperatures are likely to result in films of reduced density or changed composition, as well as decreased refractive index. It is still important to mention that the changes in refractive index values are really small, therefore no substantial changes in film quality are expected over the whole temperature range studied.

2.2. Film Structure

Figures 4 and 5 demonstrate selected X-ray diffraction (XRD) patterns of the HfO_2 films deposited at varying temperatures on glass and silicon substrates, respectively. Because the intensity of the diffraction peaks is generally higher, it can be seen that the films grown at relatively high temperatures are more crystalline. Otherwise, no particular differences between the phase contents of the films grown on both types of substrate were observed. In the films grown on ITO, the dominant peaks belonged to the $\bar{1}11$ and 111 reflections of the monoclinic phase[27] (not shown), whereas on Si substrates, the most intense reflections (such as 020 and 200), were essentially weaker in the films grown on ITO. The monoclinic HfO_2 phase was predominant in all the films, except those grown below 200 °C, where the temperature was obviously too low to initiate noticeable crystallization (Fig. 4). In the films grown on silicon, trace reflections from tetragonal or orthorhombic phases were also detected at a 2Θ value of 30.4° (Fig. 5). This is characteristic of ALD HfO_2 since similar minor reflections from metastable phases were also seen in the films grown from $HfCl_4$ and H_2O.[11,21,22]

Three films, grown at 200 °C, 250 °C, and 300 °C, were evaluated by atomic force microscopy (AFM). The AFM measurements revealed that the root-mean-square (rms) roughness of the film surface was 7.9 ± 0.4 nm, 4.6 ± 0.4 nm, and 3.7 ± 0.4 nm, respectively. The respective film thicknesses were 132 nm, 132 nm, and 170 nm. This is an interesting result because the roughness actually decreased with the increase in the deposition temperature, although, simultaneously, the crystallinity increased with the growth temperature (Fig. 5). From the AFM images of the samples grown at 200 °C and 300 °C in Figure 6, it can be seen that

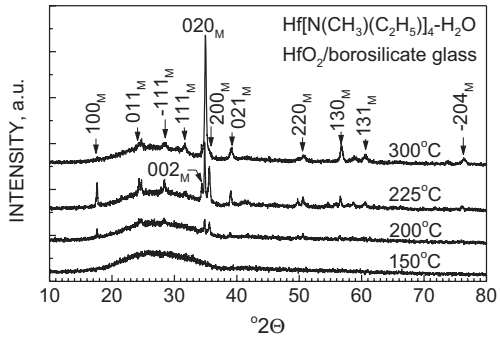

Fig. 4. XRD patterns of selected HfO_2 films grown on glass substrates. Growth temperatures are indicated by labels. Reflections are indexed as monoclinic HfO_2. The film thicknesses are 170, 200, 132, and 101 nm, for patterns counted from top to bottom.

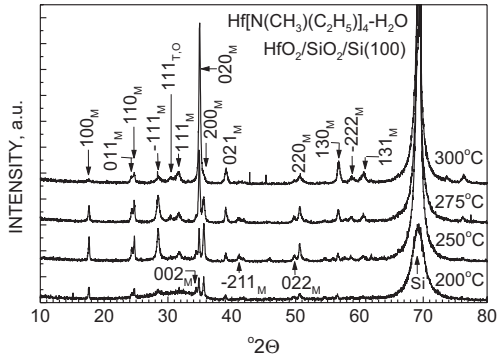

Fig. 5. XRD patterns of selected HfO_2 films grown on silicon substrates. Growth temperatures are indicated by labels. Subscripts M, T, and O at indexed reflections denote monoclinic, tetragonal, and orthorhombic phases, respectively. The film thicknesses are 170, 150, 132, and 132 nm, for patterns counted from top to bottom.

the grain size decreases considerably with the growth temperature, resulting in reduced roughness. This may be due to the increased nucleation density at 300 °C. At the same time, neither crystal size (possibly increasing with temperature and larger in the film bulk), nor film thickness affected the surface smoothness.

2.3. Film Composition

According to time-of-flight elastic recoil detection analysis (TOF-ERDA), the hafnium and oxygen concentrations were 33 ± 2 at.-% and 63 ± 2 at.-%, respectively, in the films grown in the temperature range 175–300 °C. Thus the oxygen to hafnium ratio in these samples was 2.0 ± 0.1. In the films grown at 150 °C and 325 °C, the hafnium and oxygen concentrations were 30 ± 2 at.-% and 63 ± 3 at.-%, respectively. Within the accuracy limits of TOF-ERDA, all the samples were evidently stoichiometric dioxides.

Figure 7 depicts the concentrations of residual impurities in the HfO_2 films as a function of growth temperature. In the films grown below 275 °C, carbon and nitrogen levels remained in the ranges 0.3–0.6 at.-% and 0.1–0.2 at.-%,

  0948-1907/02/0509-0201 $ 17.50+.50/0

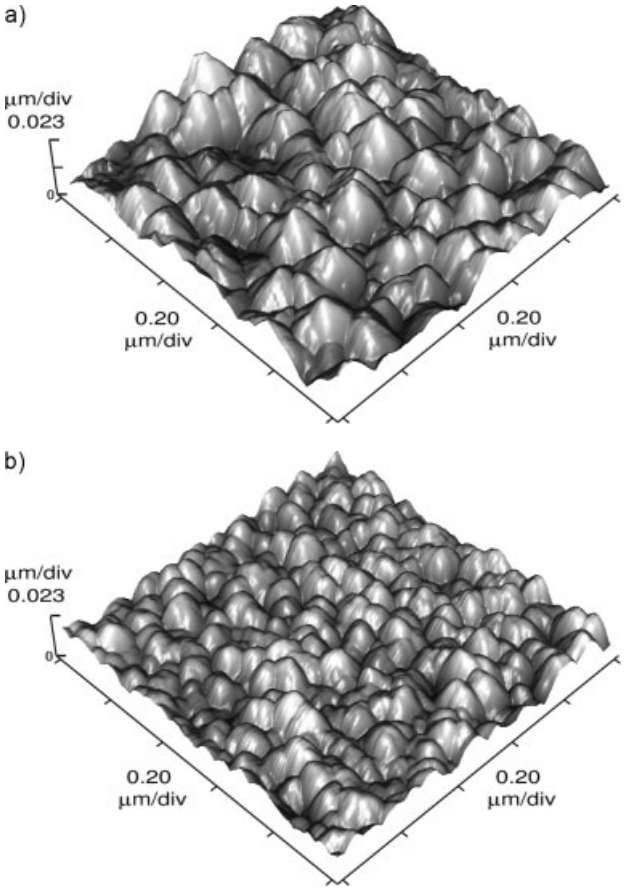

Fig. 6. AFM images of the HfO_2 films grown onto Si(100) at a) 200 °C, and b) 300 °C.

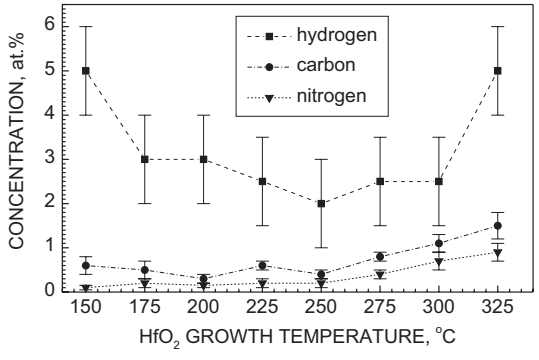

Fig. 7. Concentrations of hydrogen, carbon, and nitrogen residues versus growth temperature. Lines are guides for the eye.

respectively, whereas a slight increase in the contamination level occurred at higher deposition temperatures. The hydrogen content in the films grown in the temperature range 175–300 °C was quite stable at 2–3 at.-%, whereas increased amounts of hydrogen were found in the films grown at both lower and higher temperatures. Generally, the contaminants were distributed homogeneously throughout the film thickness. In some samples, a hydrogen peak was detected at the film surface, possibly coming from adsorbed water. Zirconium was also found in all of the HfO_2 films in concentrations not exceeding 0.2–0.4 at.-%. Zirconium is the common impurity in hafnium-based compounds and hafnium precursors.

For comparison, Ohshita et al.[19] obtained sub-stoichiometric oxides from $Hf[N(C_2H_5)_2]_4$ and O_2 in a CVD process, where the O/Hf ratio was 1.5 at a deposition temperature of 300 °C. Stoichiometric dioxides could be obtained at 350 °C. At 300 °C, the carbon impurities were strongly dependent on the O_2 dose and varied between 1 at.-% and 11 at.-%. Nitrogen content remained at the 5–7 at.-% level. Evidently, the precursors, $Hf[N(CH_3)(C_2H_5)]_4$ and H_2O, used in the ALD process in this study, enable the deposition of stoichiometric HfO_2 at lower temperatures than so far reported for alkylamide-based CVD.

2.4. Dielectric Behavior

Some capacitor structures were fabricated in order to verify the dielectric behavior of HfO_2 films grown in this study. Figure 8 demonstrates capacitance–voltage (*CV*) and dissipation behavior, measured at 500 kHz, for the films deposited at 200 °C on HF-etched Si, and at 300 °C on a Si substrate with a ca. 1.1 nm thick chemically grown SiO_2 overlayer. The film thicknesses were 133 nm and 178 nm, respectively, and the films were not heat treated before measurements. All the *CV* curves demonstrated counterclockwise hysteresis when swept from positive to negative bias forward, and from negative to positive bias backwards.

The flat-band voltage in typical Al/HfO_2/Si capacitors remains at –1 V. The *CV* curves exhibited a shift in flat-band voltage towards positive bias (Fig. 8) during the forward sweep. This is due to the intense injection of negative charge from the substrate under positive bias. The hysteresis width is noticeably larger in the films grown at lower temperature. This may be due to the (assumed to be) thinner SiO_2 interface layer, but perhaps also to the more homogeneous nature (i.e., crystalline phase dominating

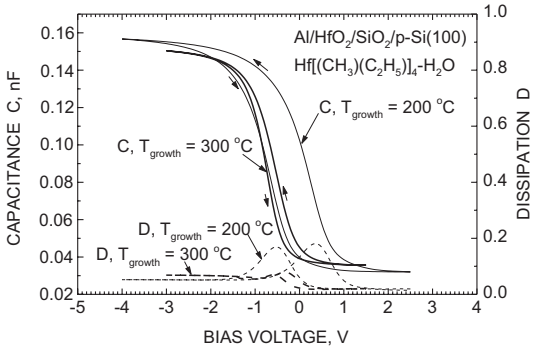

Fig. 8. Selected *CV* and dissipation curves measured for Al/HfO_2/Si capacitor structures at AC signal frequency of 500 kHz. Labels indicate HfO_2 growth temperatures. The thickness of the films grown at 200 °C and 300 °C are 133 nm and 178 nm, respectively.

  0948-1907/02/0509-0202 $ 17.50+.50/0

over an amorphous phase) of the film grown at 300 °C. The hysteresis width can be estimated using the difference between dissipation maxima occurring near flat-band conditions. The density of the oxide rechargeable traps may then be calculated from the hysteresis width.[28] For the *CV* curves depicted in Figure 8, one obtains the oxide trap densities 1.1×10^{12} cm^{-2} and 4.0×10^{12} cm^{-2} for the films grown at 300 °C and 200 °C, respectively.

The *CV* curves exhibit clear accumulation under strongly negative bias voltage. The effective permittivity of the dielectric oxide layer(s) can be calculated from the accumulation capacitance by using the simple parallel plate capacitor model. This gives effective permittivity values of 11.3 ± 0.5 and 14.5 ± 0.5 for the HfO_2 films grown at 200 °C and 300 °C, respectively. In the latter case, the effect of the 1.1 nm SiO_2 interface layer has been taken into account by using the series connection of parallel plate capacitors with SiO_2 and HfO_2 dielectric layers.

The permittivity values calculated for the Al/HfO_2/ITO capacitors compared favorably with the effective permittivities of the films on silicon. The sample films were deposited on ITO at arbitrarily chosen temperatures of 205 °C and 250 °C. The corresponding film thicknesses were 135 nm and 127 nm. The respective permittivities were 12.3 ± 0.3 and 14.0 ± 0.1, independent of the measurement frequency (varied between 10 kHz and 500 kHz).

The current–voltage behavior of these capacitors was also examined. The leakage current density versus electric field curves (not shown) demonstrated that the current density remained below 1×10^{-5} A cm^{-2} until the dielectric breakdown. Typically, the breakdown occurred at 2.5–2.6 MV cm^{-1} and 2.8–2.9 MV cm^{-1} in the Al/HfO_2/ITO capacitors with dielectric layers grown at 250 °C and 205 °C, respectively. The difference in the breakdown resistance in the films grown at higher temperature can be explained by somewhat higher polycrystallinity and some contribution from the grain boundary conductivity. In the Al/HfO_2/Si capacitors, the breakdown occurred at 3.5 MV cm^{-1} and 3.7 MV cm^{-1} with dielectric layers grown at 200 °C and 300 °C. At 300 °C, the film was grown onto 1.1 nm SiO_2 formed on Si(100) and this can give rise to breakdown resistance. In these particular samples, the pre-breakdown leakage current was between 1×10^{-6} A cm^{-2} and 1×10^{-5} A cm^{-2} in the field range 2.0–3.5 MV cm^{-1} measured for the film grown at 200 °C, whereas for the film grown at 300 °C, the pre-breakdown current remained between 1×10^{-7} A cm^{-2} and 5×10^{-7} A cm^{-2} in the electric field range 2.0–3.7 MV cm^{-1}. More detailed study on the dielectric properties is beyond the scope of the present paper. Possible formation and effect of interface layers on HF-etched Si, as well as its increase during deposition and storage in ambient air, remains a matter for future investigation. Further, the effect of growth and annealing temperatures, film thickness, and structure on the permittivity and interface quality should also be studied.

3. Summary

Stoichiometric HfO_2 films can be grown by ALD from $Hf[N(CH_3)(C_2H_5)]_4$ and H_2O in the temperature range 150–325 °C. The adsorption of $Hf[N(CH_3)(C_2H_5)]_4$ is a self-limiting process, as confirmed at 250 °C. In the temperature range 200–250 °C, the film growth is quite independent of the growth temperature. The growth rate and residual hydrogen contamination increase towards both lower and higher temperatures outside this range. The hydrogen concentration at 200–500 °C was 2–3 at.-%. The carbon and nitrogen concentrations were 0.3–0.6 at.-% and 0.1–0.2 at.-%, respectively, increasing somewhat with the deposition temperature. The films crystallize when growing at temperatures exceeding 150–175 °C. The refractive index of the HfO_2 films grown on glass substrates was 2.08–2.10. The dominant phase in the films is monoclinic HfO_2 with a somewhat preferred (020) texture on Si(100) and glass, and with most intense $\bar{1}11$ and (111) orientations when grown on polycrystalline ITO. The effective permittivities of HfO_2 in Al/HfO_2/Si capacitor structures were 11.3 and 14.5, measured for the films grown at 200 °C and 300 °C, respectively. The permittivities of HfO_2 in Al/HfO_2/ITO capacitor structures were 12.3 and 14.0, measured for the films grown at 205 °C and 250 °C, respectively. The breakdown in HfO_2 films occurred at 2.6–2.9 MV cm^{-1} in the films grown on ITO, and at 3.53.7 MV cm^{-1} in the films grown on Si.

4. Experimental

The films were grown in a hot-wall horizontal flow-type ALD reactor [29] onto borosilicate glass, Si(100), and glass substrates covered by patterned ITO electrodes. The substrate temperature was varied in the range 150–325 °C. The pressure in the reactor was about 10 mbar. $Hf[N(CH_3)(C_2H_5)]_4$ [30] (Aldrich, 99.99+ %, product number 553 123) was evaporated from an open boat at 60 °C inside the reactor. H_2O vapor was generated in an external reservoir at room temperature and led into the reactor through needle and solenoid valves. Metal precursor pulse length was varied between 0.2 s and 1.0 s, while the water pulse length was held at 0.5 s. Constant purge times of 0.5 s were used after each precursor pulse to separate the precursor flows in the gas phase and to remove the excess reactants and gaseous reaction by-products from the system. Nitrogen was used as both precursor carrier and purge gas.

The film thickness and optical properties were calculated from optical transmission spectra [31] measured by a Hitachi U-2000 spectrophotometer. The structure of the films was determined by means of a Philips MPD 1880 powder X-ray diffractometer using Cu Kα radiation and the Bragg–Brentano geometry. The surface roughness of some selected samples was evaluated using a ThermoMicroscopes CP Research AFM. The film composition and residual contamination level were evaluated by TOF-ERDA [32]. A 53 MeV $^{127}I^{10+}$ beam for TOF-ERDA was obtained from a 5 MV tandem accelerator EGP-10-II, and forward scattered iodine ions and recoiled target atoms were used for the determination of Hf and lighter elements, respectively. Dielectric properties were measured after e-beam evaporation of aluminum electrodes with an effective electrode area of 0.204 mm^2. After film deposition, the reverse of the silicon substrates were etched in hydrofluoric acid and metallized by evaporating a 100 nm thick Al layer. Thus, the electrical measurements were carried out on Al/HfO_2/p-Si(100)/Al, Al/HfO_2/SiO_2/p-Si(100)/Al, or Al/HfO_2/ITO capacitor structures. *CV* curves were recorded using a HP 4284A precision LCR meter. The stair-sweep voltage step was 0.05 V, and the period between voltage steps was 0.5 s. The AC

  0948-1907/02/0509-0203 $ 17.50+.50/0

voltage applied to the capacitor was 0.05 V or 0.005 V while the frequency of the AC signal was held at either 100 kHz or 500 kHz. The current–voltage curves were measured with a Keithley 2400 Source Meter in the stair-sweep voltage mode, while the voltage step used was 0.02–0.05 V. All measurements were carried out at room temperature.

Received: December 19, 2001
Final version: March 18, 2002

[1] S. A. Campbell, T. Z. Ma, R. Smith, W. L. Gladfelter, F. Chen, *Microelectron. Eng.* **2001**, *59*, 361.
[2] E. P. Gusev, E. Cartier, D. A. Buchanan, M. Gribelyuk, M. Copel, H. Okorn-Smith, C. D'Emic, *Microelectron. Eng.* **2001**, *59*, 341.
[3] L. Peters, *Semicond. Int.* **2001**, *24*, 61.
[4] T. Kanniainen, H. Kattelus, J. Skarp, *Electrochem. Soc. Proc.* **1997**, *97-31*, 36.
[5] S. Capone, G. Leo, R. Rella, P. Siciliano, L. Vasanelli, M. Alvisi, *J. Vac. Sci. Technol. A* **1998**, *16*, 3564.
[6] C. L. Platt, B. Dieny, A. E. Berkowitz, *Appl. Phys. Lett.* **1996**, *68*, 2291.
[7] M. Alvisi, M. Di Giulio, S. G. Marrone, M. R. Perrone, M. L. Protopapa, A. Valentini, L. Vasanelli, *Thin Solid Films* **2000**, *358*, 250.
[8] W.-J. Qi, B. H. Lee, R. Nieh, L. Kang, Y. Jeon, K. Onishi, J. C. Lee, *Proc. SPIE—Int. Soc. Opt. Eng.* **1999**, *3881*, 24.
[9] A. N. Saxena, K. L. Mittal, *J. Appl. Phys.* **1975**, *46*, 2788.
[10] J. G. Bendoraitis, R. E. Salomon, *J. Phys. Chem.* **1965**, *69*, 3666.
[11] M. Ritala, M. Leskelä, L. Niinistö, T. Prohaska, G. Friedbacher, M. Grasserbauer, *Thin Solid Films* **1994**, *250*, 72.
[12] B. H. Lee, L. Kang, R. Nieh, W.-J. Qi, J. C. Lee, *Appl. Phys. Lett.* **2000**, *76*, 1926.
[13] M. Fadel, O. A. Azim, O. A. Omer, R. R. Basily, *Appl. Phys. A—Mater. Sci. Process.* **1998**, *66*, 335.
[14] J. Leng, S. Li, J. Opsal, D. Aspnes, B. H. Lee, J. Lee, *Proc. SPIE—Int. Soc. Opt. Eng.* **2000**, *4099*, 228.
[15] Z. Czigány, D. Mademann, P. Weißbrodt, E. Hacker, *Solid State Phenom.* **1997**, *56*, 233.
[16] M. Balog, M. Schrieber, S. Patai, M. Michman, *J. Cryst. Growth* **1972**, *17*, 298.
[17] M. Balog, M. Schrieber, M. Michman, S. Patai, *Thin Solid Films* **1977**, *41*, 247.
[18] R. C. Smith, T. Ma, N. Hoilien, L. Y. Tsung, M. J. Bevan, L. Colombo, J. Roberts, S. A. Campbell, W. L. Gladfelter, *Adv. Mater. Opt. Electron.* **2000**, *10*, 105.
[19] Y. Ohshita, A. Ogura, A. Hoshiro, S. Hiiro, H. Machida, *J. Cryst. Growth* **2001**, *233*, 292.
[20] Y. Ohshita, A. Ogura, A. Hoshino, T. Suzuki, S. Hiiro, H. Machida, *J. Cryst. Growth* **2002**, *235*, 365.
[21] J. Aarik, A. Aidla, A.-A. Kiisler, T. Uustare, V. Sammelselg, *Thin Solid Films* **1999**, *340*, 110.
[22] J. Aarik, A. Aidla, H. Mändar, T. Uustare, K. Kukli, M. Schuisky, *Appl. Surf. Sci.* **2001**, 173, 15.
[23] K. Kukli, J. Ihanus, M. Ritala, M. Leskelä, *Appl. Phys. Lett.* **1996**, *68*, 3737.
[24] K. Forsgren, Comprehensive Summaries of Uppsala Dissertations from the Faculty of Science and Technology, 665, *Acta Univ. Upsaliensis* **2001**, p. 37.
[25] R. G. Gordon, J. Becker, D. Hausmann, S. Suh, *Chem. Mater.* **2001**, *13*, 2463.
[26] J. Wang, H. P. Li, R. Stevens, *J. Mater. Sci.* **1992**, *27*, 5397.
[27] International Centre for Diffraction Data (ICDD), Newtown Square, PA, Powder Diffraction File, card 43-1017.
[28] D. K. Schröder, *Semiconductor Material and Device Characterization*, 2nd ed., J. Wiley and Sons, Inc., New York **1998**. p. 350.
[29] T. Suntola, *Thin Solid Films* **1992**, *216*, 84.
[30] R. G. Gordon, *Electrochem. Soc. Proc.* **2000**, *13*, 248.
[31] M. Ylilammi, T. Ranta-aho, *Thin Solid Films* **1993**, *232*, 56.
[32] J. Jokinen, P. Haussalo, J. Keinonen, M. Ritala, D. Riihelä, M. Leskelä, *Thin Solid Films* **1996**, *289*, 159.

  0948-1907/02/0509-0204 $ 17.50+.50/0